ACS OMEGA

Open Access

http://pubs.acs.org/journal/acsodf

Article

Fabrication of Bilayer Nanofibrous-Hydrogel Scaffold from *Bacterial Cellulose*, *PVA*, and *Gelatin* as Advanced Dressing for Wound Healing and Soft Tissue Engineering

Rawaiz Khan, Muhammad Umar Aslam Khan,* Goran M. Stojanović, Aneela Javed, Sajjad Haider, and Saiful Izwan Abd Razak*

Cite This: *ACS Omega* 2024, 9, 6527−6536

Read Online

ACCESS | Metrics & More | Article Recommendations

ABSTRACT: Tissue engineering is currently one of the fastest-growing areas of engineering, requiring the fabrication of advanced and multifunctional materials that can be used as scaffolds or dressings for tissue regeneration. In this work, we report a bilayer material prepared by electrospinning a hybrid material of poly(vinyl alcohol) (PVA) and bacterial cellulose (BC NFs) (top layer) over a highly interconnected porous 3D gelatin-PVA hydrogel obtained by a freeze-drying process (bottom layer). The techniques were combined to produce an advanced material with synergistic effects on the physical and biological properties of the two materials. The bilayer material was characterized using Fourier transform infrared spectroscopy (FTIR), scanning electron microscopy (SEM), and a water contact measurement system (WCMS). Studies on swelling, degradability, porosity, drug release, cellular and antibacterial activities were performed using standardized procedures and assays. FTIR confirmed cross-linking of both the top and bottom layers, and SEM showed porous structure for the bottom layer, random deposition of NFs on the surface, and aligned NFs in the cross section. The water contact angle (WCA) showed a hydrophilic surface for the bilayer material. Swelling analysis showed high swelling, and degradation analysis showed good stability. The bilayer material released Ag-sulfadiazine in a sustained and controlled manner and showed good antibacterial activities against severe disease-causing gram + ive and −ive (*Escherichia coli*, *Staphylococcus aureus*, and *Pseudomonas aeruginosa*) bacterial strains. In vitro biological studies were performed on fibroblasts (3T3) and human embryonic kidneys (HEK-293), which showed desirable cell viability, proliferation, and adhesion to the bilayer. Thus, the synergistic effect of NFs and the hydrogel resulted in a potential wound dressing material for wound healing and soft tissue engineering.

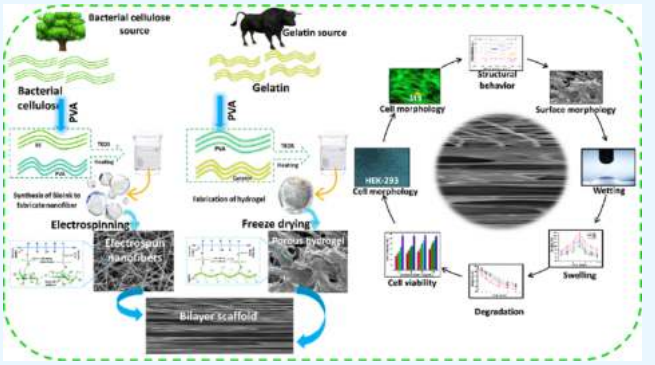

1. INTRODUCTION

Skin wound healing is a complex process involving numerous biological and physiological factors. It is a typical biological response to harm and is essential to maintain the health and operation of the underlying tissues and skin.[1,2] Tissue engineering (TE) is a cutting-edge method for treating damaged tissues using bioactive substances as scaffolds for cell immobilization to encourage tissue regeneration and healing. Scaffolds are the three-dimensional (3D) structural framework that promotes cell proliferation, migration, and adhesion.[3,4] Scaffolds can be fabricated from synthetic and natural polymers and serve as templates for developing new tissue. They can release growth factors or bioactive compounds that help in wound healing. For efficient wound healing, scaffolds with specified properties, such as biocompatibility, biodegradability, and regulated porosity, are needed.[5] The TE techniques for skin wound healing have shown encouraging outcomes and have been used for skin injuries, burns, and persistent wounds.

Natural polymer-based hydrogels are frequently employed in the treatment of wounds. Hydrogels are similar to human tissues in absorbing water.[6] Hydrogels are breathable, soft, and flexible, preserving moisture, promoting cell proliferation, and allowing the delivery of nutrients and oxygen to the wound site.[7,8] They develop an environment suitable for repairing, regenerating, and wound healing applications. Because hydrogels are biocompatible, biodegradable, and resemble the

Received: September 6, 2023
Revised: December 16, 2023
Accepted: December 27, 2023
Published: February 1, 2024

Scheme I. Synthesis of Nanofiber and Hydrogels from Gelatin, Bacterial Cellulose, and Tetraethyl Orthosilicate to Fabricate Nanofibrous Bioscaffolds for Wound Healing Applications

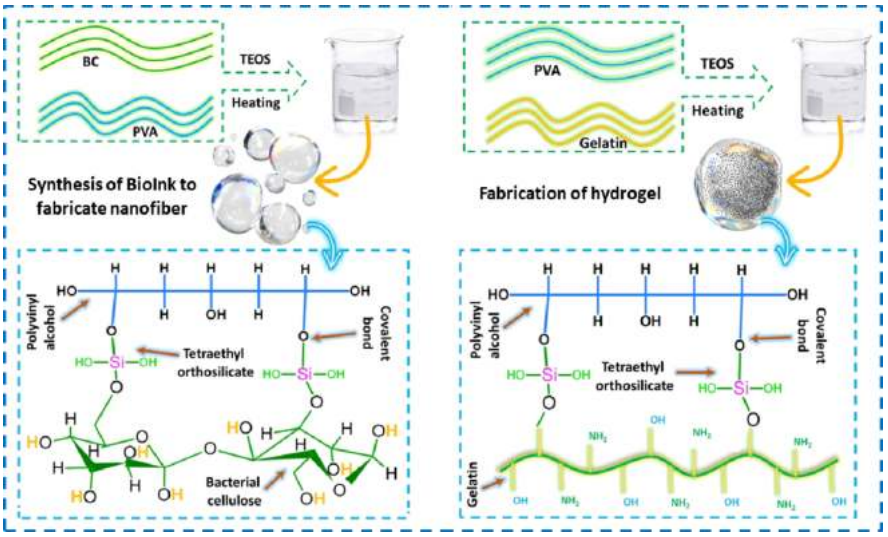

extracellular matrix (ECM), gelatin-based hydrogels are prospective biomaterials for use in the treatment of wounds.[9] The 3D structure of freeze-dried biomaterials encourages cell adhesion, migration, and proliferation, promoting tissue regeneration.[10,11] They can absorb and hold a large amount of water, resulting in a moist environment that supports wound healing. For long-lasting therapeutic benefits at the site of the wound, the 3D matrix may function as storage that releases bioactive chemicals.

Bacterial cellulose (BC) is a biocompatible polysaccharide with the potential to be used in biomedicine and has attracted a great deal of attention for wound healing applications. Like other hydrogels, BC-based hydrogels have a highly porous structure, water-holding capacity, and biodegradability but are distinct in having good mechanical integrity.[12,13] Due to its distinctive fibrous structure, cells can cling to it, migrate over it, and proliferate therein, aiding tissue regeneration. BC-based hydrogels have high gas permeability, which enables the exchange of gases (O_2 and CO_2), nutrients, and waste throughout the wound site and the surrounding environment.[14] BC hydrogels are frequently made into pliable, flexible dressings, which make them simple to handle and apply to wounds of many sizes and forms. Since BC hydrogels are similar to ECM, they are considered good for promoting cell infiltration, nutrient transport, and tissue regeneration.[3,15] As discussed, gelatin-based and BC materials showed their potential for wound healing application. However, the gelatin-based scaffolds' instability and weak mechanical strength can be controlled by tailoring them with other polymers and designing the architecture of the scaffolds. Human Embryonic Kidney (HEK-293) is a cell line commonly used for BioPharma, basic medical research, and therapeutic solutions. They were generated in 1973 and are derived from human embryonic kidney cells. They are very popular and have been used in various studies due to their reliable growth in culture, from basic research to studying the biocompatibility of the materials produced.[16] Luchi et al. used the cell line to study the biocompatibility of nanocomposites because of their potential application in tissue engineering.[17] In a similar study, Plange et al. used HEK 293 to investigate the cytocompatibility of gelatin scaffolds for tissue engineering.[18]

In this study, we report the development of novel nanofibrous bilayer scaffolds with gelatin-PVA as a hydrogel (bottom layer) produced via freeze-drying and BC-PVA as a nanofiber (top layer) produced via electrospinning. FTIR and SEM were used to determine their structural and morphological properties. Wetting, swelling, degradation, water retention, and porosity were determined by using standard procedures. Cell morphology and viability of the fibroblast (*3T3*) and Human Embryonic Kidney (*HEK-293*) were determined using standard assays. The antibacterial activities were determined against Gram (+ive and −ive) bacterial strains. The bilayer hydrogel-nanofibrous scaffolds had interconnected pores, allowing efficient fluid absorption and cell migration, facilitating nutrient diffusion, supporting tissue ingrowth, tissue integration, and good antibacterial activity, and the high surface area facilitated cell attachment.

2. MATERIALS AND METHODS

2.1. Materials. BC was extracted, as reported in our previous studies by Khan et al.[3] Gelatin (CAS no. G9382-500G), tetraethyl orthosilicate (TEOS) (CAS no. 78-10-4), phosphate buffer saline (PBS), absolute ethanol (C_2H_5OH), glacial acetic acid (CH_3OOH), potassium persulfate (KPS), Triton X-100, calcium chloride ($CaCl_2$), and sodium chloride (NaCl) were purchased from Sigma-Aldrich. The fibroblast (*3T3*) and Human Embryonic Kidney (*HEK-293*) cell lines were provided by the American Type Culture Collection (ATCC). Live/dead cell culture staining was purchased from Gibco. Fetal bovine serum (FBS) and antibiotics (penicillin and streptomycin) containing Dulbecco's modified Eagle's medium (DMEM)) were supplied by Molecular Probes. The cell morphology of the *3T3* cell line was evaluated by a live/dead assay kit (Invitrogen−R37601). The live/dead assay kit contains components A and B (Calcein-AM (green) and BOBO-3 Iodide (red)). These were mixed in the assay kits and filled in the cell culture wells with an equal quantity of the serum-free medium.

2.2. Methods. *2.2.1. Fabrication of 3D Sponge.* The porous interconnected 3D gelatin-PVA hydrogel was fabricated via a freeze-drying technique. A 0.7 g amount of gelatin was dispersed in 10 mL of double deionized water (DDW) and 0.3

https://doi.org/10.1021/acsomega.3c06613
ACS Omega 2024, 9, 6527−6536

g amount of PVA was heated in 10 mL of DDW at 80 °C to have polymeric solutions. Both polymeric solutions were mixed at 60 °C for 1 h to homogenized solution. Then, a series of hydrogels were prepared by adding different amounts (30, 60, 90, and 120 μL) of tetraethyl orthosilicate (TEOS) to the homogeneous mixture at 60 °C for 3 h to cross-link the hydrogels. The KPS (0.1 g) was added to the suspension as an initiator, which changed the color of the mixtures from yellowish to off-white. After 3 h, the hydrogels with different cross-linking were poured into Petri plates and kept at 20 °C by covering paraffin tape and freeze-dried under a vacuum to get a porous 3D polymeric matrix. The well-dried 3D polymeric matrixes were coded as Gel: PVA-30, Gel: PVA-60, Gel: PVA-90, and Gel: PVA-120. The coding corresponded to the amounts of cross-linker (30, 60, 90, and 120 μL). The schematic diagram (SchemeI) summarizes the proposed chemical reaction.

2.3. Fabrication of Nanofiber. The BC and PVA polymeric solutions were prepared by adding 0.7 g of BC into 15 mL and 0.3 g of PVA into 10 mL of DDW. These polymeric solutions were mixed and stirred for 1 h at 60 °C to have homogenized polymeric solutions of BC-PVA. Then, a series of solutions were prepared by adding different amounts of TEOS (60, 120, 180, and 240 μL) first into 5 mL of ethanol and then dropwise into polymeric solution, followed by the addition of KPS (0.1 g) that converted solutions color from yellowish to off-white. The solutions were allowed to be stirred for 3 h at 60 °C to produce BioInk with different cross-linking. Then, the BioInk of BC-PVA was fed into the syringe with a 24G needle and electrospun over the aluminum foil at the collector. The high electric potential of 4 kV/cm was applied between the syringe and collector by keeping a distance of 15 cm. The flow rate of BioInk was kept at 1 mL/h by a controlled syringe pump. The high-voltage DC power supply was used by connecting the positive terminal to a 24G needle and the negative terminal to the collector. The nanofibers were collected from collectors for further characterization. The well-dried nanofibers were coded (BC: PVA-60, BC: PVA-120, BC: PVA-180, and BC: PVA-240). The coding corresponded to the amounts of cross-linker (60, 120, 180, and 240 μL). The proposed chemical interaction is shown in the schematic illustration (SchemeI).

2.4. Fabrication of Nanofibrous Bioscaffolds. The cross-linked BC: PVA-120, due to its better spinnability and smooth fiber morphology, was finalized to produce nanofibers over the already produced 3D porous hydrogels. These 3D porous hydrogels were placed over the aluminum substrate, which is attached to the collector, and electrospun to get nanofibrous bilayer scaffolds (NBS-1, NBS-2, NBS-3, and NBS-4) under the above-mentioned parameters. The fabricated 3D nanofibrous bioscaffolds were stored at room temperature for further analysis.

3. CHARACTERIZATIONS

The structural and functional group analysis of the bilayer hydrogel-nanofibrous scaffolds was studied using Fourier-transform infrared spectroscopy (Nicolet 6700, Waltham, MA, United States). The FTIR spectral resolution was kept at 4 cm^{-1}, and the frequency ranged from 4000 to 500 cm^{-1}. The surface morphology of bilayer hydrogel-nanofibrous scaffolds was studied using SEM (JEOL-JSM 5410 LV). Before the SEM analysis, bilayer hydrogel-nanofibrous scaffolds were well-dried under a vacuum to avoid moisture and then gold-sputtered. The wettability of the bilayer hydrogel-nanofibrous scaffolds was conducted using a water contact meter system (JY-82, Dingsheng, Chengde, China).

3.1. Swelling, Degradation, Water retention and Porosity Analysis. The swelling behavior of the bilayer hydrogel-nanofibrous scaffolds was evaluated in DDW, PBS, and NaCl media with different pH ranges at 37 °C. The 1 × 1 cm^2 pieces of bilayer hydrogel-nanofibrous scaffolds were kept in the media mentioned above. After a specific interval, the swollen bilayer hydrogel-nanofibrous scaffolds were removed from the corresponding media. The surface water was carefully removed with a tissue. Equation 1 was used to calculate the swelling percentage by using the weight of bilayer hydrogel-nanofibrous scaffolds before swelling (W_o) and after swelling (W_f).

$$\text{Swelling}\ (\%) = \frac{W_S - W_O}{W_O} \times 100 \tag{1}$$

The bilayer hydrogel-nanofibrous scaffold was degraded in PBS media (7.4 pH, 37 °C). The well-dried bilayer hydrogel-nanofibrous scaffolds (W_i) were cut into square form and weight (50 mg), placed into PBS media, and taken out after a specific time, "*t*," to record the weight (W_t). Equation 2) was used to calculate the degradation of the bilayer hydrogel-nanofibrous scaffolds. Similary the water retention behavior of the nanofibrous bilyer scaffolds was determined.

$$\text{Weight loss}\ (\%) = \frac{W_i - W_t}{W_i} \times 100 \tag{2}$$

The porosity of bilayer hydrogel-nanofibrous scaffolds was evaluated using the liquid displacement method and taking ethanol as displacement media due to its nonswelling, nondegradation, and easy penetration approaches. The bilayer hydrogel-nanofibrous scaffolds were weighed (W) before analysis and kept in the ethanol-containing cylinder with known volume (V_1) for 5 min. Then, evacuation−pressurization cycles were performed that forced ethanol to get into the pores of bilayer hydrogel-nanofibrous scaffolds, and this process was repeated until the air bubble stopped and the total volume was recorded (V_2). The bilayer hydrogel-nanofibrous scaffolds were removed from the cylinder, the volume was taken as V_s, and the porosity was determined by following equation:

$$\text{Porosity} = \frac{V_1 - V_S}{V_2 - V_S} \times 100 \tag{3}$$

W_i is the initial weight, W_f is the final weight, and W_t is the weight at "*t*" time. V_1 is the ethanol volume, V_2 is the ethanol and sample volume, and V_s is the sample volume.

3.2. In Vitro Assays. *3.2.1. Drug Delivery.* The silver-sulfadiazine (Ag-sulfadiazine) is a famous antibacterial medicine and has been extensively studied as a model drug in wound healing and other biomedical applications. It was loaded into the bilayer hydrogel-nanofibrous scaffolds. Briefly, Ag-sulfadiazine (25 mg) was dissolved in methanol and added dropwise to the polymeric solution of Gelatin-PVA. The drug-containing polymeric system was stirred for 1 h for a homogenized solution. Cross-linking was carried out using the same method as mentioned above. The cross-linked drug-loaded solution was poured into Petri plates, frozen at −80 °C, and freeze-dried at −40 °C to get 3D hydrogels. The BC-PVA nanofiber layer was produced on the 3D hydrogels as described

https://doi.org/10.1021/acsomega.3c06613
ACS Omega 2024, 9, 6527−6536

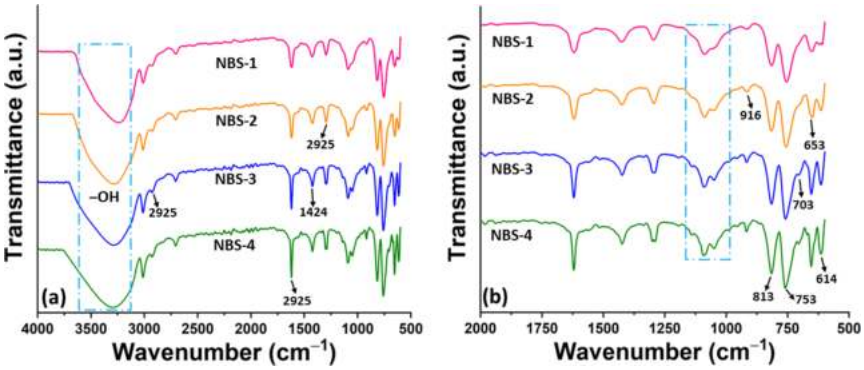

Figure 1. FTIR spectral profile of nanofibrous bioscaffolds, (a) spectral profile of the nanofibrous scaffolds from 4000 to 400 cm^{-1} and (b) spectral prolife of nanofibrous scaffolds from 2000 to 500 cm^{-1}.

above. The bilayer hydrogel-nanofibrous scaffolds were placed into a beaker containing PBS (100 mL) at 37 °C, and a 2 mL sample was taken after 10 min. The sample was run in a UV−vis spectrometer at 297 nm, and the solution was refilled with the same medium to maintain the solution volume. The PBS medium was taken as a reference, and the drug release was calculated using a calibration graph.

3.2.2. Antibacterial Activities. The antibacterial activities of the bilayer hydrogel-nanofibrous scaffolds containing Ag-sulfadiazine were evaluated against Gram-negative (*Pseudomonas aeruginosa* (*P. aeruginosa*), *Escherichia coli* (*E. coli*)) and Gram-positive (*Staphylococcus aureus* (*S. aureus*)) bacterial strains by disc diffusion method. The antibacterial behavior of the bilayer hydrogel-nanofibrous scaffolds was determined by zone inhibition. The molten agar was poured into the Petri dish and allowed to settle, and then, bacterial strains were applied uniformly with a sterilized glass spreader. The bacterial media was spotted with 70 μL of equally homogenized bilayer hydrogel-nanofibrous scaffolds and incubated for 12 h at 37 °C. Finally, the antibacterial activity of each sample was recorded by measuring the bacterial zone inhibition.

3.2.3. Hemocompatibility. The hemocompatibility of the homogenized bilayer hydrogel-nanofibrous scaffolds was evaluated with fresh human blood. The fresh blood was heparinized. PBS was used for dilution. Different concentrations of bilayer hydrogel-nanofibrous scaffolds were employed by incubating them at 37 °C for 2 h in an incubator shaker. The fresh blood was treated with positive and negative controls using 500 μL of Triton X-100 and PBS, respectively. The incubated samples were centrifuged for 10 min at 5000 rotations per minute (rpm). The supernatants were then collected, and their absorbance was recorded at 540 nm. The hemolysis was calculated using the following equation:

$$\text{Hymolysis (\%)} = \frac{A_S - A_{NC}}{A_{PC} - A_{NC}} \times 100 \quad (4)$$

A_S is the sample absorbance, A_{PC} is positive controls, and A_{NC} is negative control.

The blood coagulation time is the time taken to clot the fresh blood. Fresh human blood was taken in a citrated vacutainer tube. It is recalcified with 5 μL of 0.05 M calcium chloride solution. The fresh blood was treated with different concentrations (50−200 μg/mL) of bilayer hydrogel-nanofibrous scaffolds at 37 °C, and the blood flow was recorded.

3.2.4. Cell Viability. The cell viability of bilayer hydrogel-nanofibrous scaffolds was evaluated against fibroblast (*3T3*) and Human Embryonic Kidney (*HEK-293*) cell lines under standard in vitro conditions (5% CO_2, 90% humidity at 37 °C). The cell viability was evaluated against different concentrations (1.0−2.5 μg/mL) of bilayer hydrogel-nanofibrous scaffolds using both cell lines for different times (24, 48, and 72 h). The bottom of the well plate was coated with 0.1% gelatin media, taken as a positive control after cell culture and incubated for 2 h using the Neutral Red method reported by Repetto et al.[19] Then, the well plates were washed with PBS media to wash additional NR media, and the cell viability was calculated using the following equation:

$$\text{Cell viability (\%)} = \frac{OD_S}{OD_C} \times 100 \quad (5)$$

OD_s is the optical density of sample and OD_C is the optical density of control.

3.2.5. Cell Culture and Morphology. The fibroblast (*3T3*) and Human Embryonic Kidney (*HEK-293*) cell lines were seeded to observe their cellular behavior against the newly developed formulations. The fine coating of gelatin (0.1%) was applied on the bottom of 24 well plates in triplicate sterilized by using UV for 1 h. Then, the *3T3* and *HEK-293* cell lines were cultured with a density of 5000 cells/cm^2 in the 24-well plates in the presence of antibiotics (streptomycin/penicillin), DMEM, and FBS to culture cell lines. The cell-cultured 24-well plates were incubated at different intervals (24, 48, and 72 h). The cell morphologies *3T3* were observed by a live/dead assay kit filled with an equal amount of well-mixed A and B and serum-free medium (50 μL). The well plates were incubated under standard in vitro conditions for 30 min. A Nikon Eclipse TS100 inverted microscope was employed to observe the cell morphologies of 3T3 and HEK-293.

3.3. Statistical Analysis. The statistical analysis of the obtained data was studied using SPSS (SPSS, Inc. V 21, USA) and one-way ANOVA. The post hoc (Tukey) tests with comparisons were used (*$p < 0.05$, **$p < 0.01$, and ***$p < 0.001$ size of sample $n = 3$).

4. RESULTS AND DISCUSSIONS

4.1. FTIR Analysis. Figure 1 shows the FTIR spectra used to investigate the changes in the chemical structure of the bilayer hydrogel-nanofibrous scaffold. The spectra exhibit different vibrational bands. The broadband at 3600−3200 cm^{-1} is attributed to the hydrogen-bonded −OH functionality. The −OH functionality is abundantly available in BC, Gelatin, and PVA. The slight difference in the broadness of the bands

https://doi.org/10.1021/acsomega.3c06613
ACS Omega 2024, 9, 6527−6536

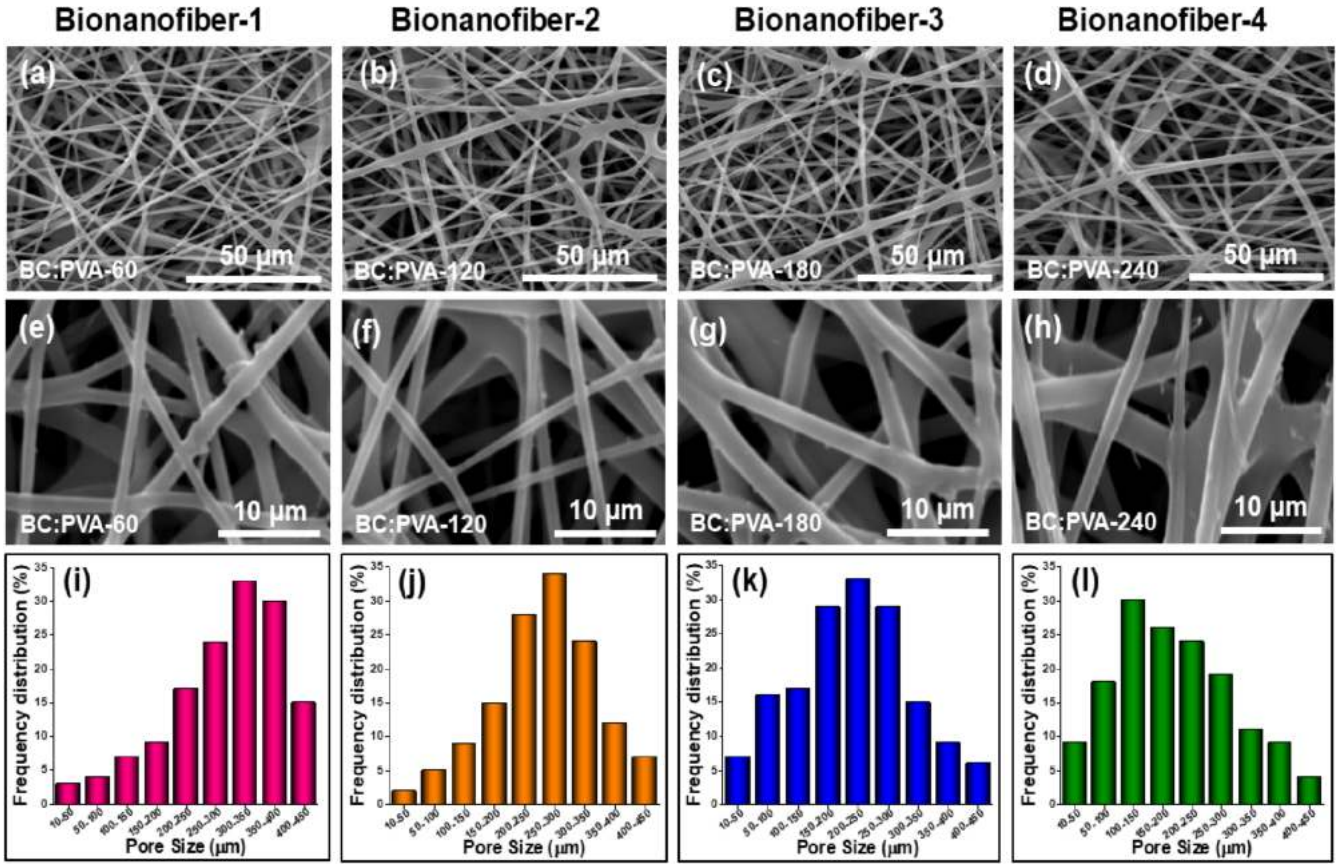

Figure 2. SEM morphology of the bionanofiber at different scales 50 (a−d) and 10 μm (e−h). ImageJ analyzed the pore size distribution (i−l).

for the bonded −OH functionality is attributed to the difference in cross-linking due to the difference in the cross-linker (TEOS) concentrations. The vibration bands at 1194 cm^{-1}, 1047 cm^{-1}, and 988 cm^{-1} confirmed the presence of C−O stretching, polysaccharide pyranose ring, and O−H bending vibration, respectively.[3] These are the characteristics of the functional bands of BC and gelatin. The absorption bands at 1424 and 1091 cm^{-1} are attributed to the −OH bending and C═O stretching functionalities of the PVA and gelatin, respectively.[20] The vibration bands at 2925 and 1619 cm^{-1} are attributed to $-CH_2$ and −OH functionalities, respectively. The band at 1619 cm^{-1} is attributed to intermolecular hydrogen bonding in water molecules. The −Si−O−C and −Si−O−Si functionalities were confirmed by the appearance of the band in the range of 1130−1000 cm^{-1}. Appearance of the band in this range confirms the cross-linking of BC-PVA and Gelatin-PVA via the silanol functionality.[21] The presence of the characteristic bands of the components in the spectra of bilayer hydrogel-nanofibrous scaffolds confirmed the successful fabrication of the target material.

4.2. Nanofibers SEM Analysis. Figure 2 shows the surface morphologies of the electrospun BC-PVA bionanofibers with different degrees of cross-linking. The bionanofibers showed smooth, bead-free morphologies with a good pore size distribution (with a pore size in the range of 300−350 μm). Cross-linking did not show much effect on the fiber morphology, but the pore size distribution of the mesh is slightly decreased (with a pore size in the range of 100−150 μm) when the concentration of the cross-linker (TEOS) is increased from 60 to 240 μL. A slight change in the morphology of the nanofibers was also observed with an increase in the amount of TEOS. These nanofibers may offer varying surface areas and pore sizes that may offer different microenvironments for cell adhesion and proliferation. It could promote soft tissue healing in TE applications.[22] Therefore, the nanofibrous substrate with smooth and bead-free nanofibers, adequate porous surface, surface roughness, and good surface area supports improved cellular behavior (adhesion and proliferation),[23] promoting wound healing in biomedical engineering.

4.3. Morphological Analysis. BC: PVA-120 was selected to fabricate nanofibers on gelatin PVA-based 3D hydrogels based on the pore size distribution and morphological observations. The top layer is the BC: PVA-120 nanofiber layer (Figure 3 (a−d)), and the bottom layer is the porous hydrogel (Figure 3 (e−h)). The bottom layer shows the surface morphology of the porous hydrogel at different cross-linking degrees. The top layer of the bilayer nanofibrous hydrogels shows a well-organized, uniform, and smooth nanofibrous phase. In contrast, the bottom layer represents the highly cross-linked and 3D porous spongy-like hydrogel phase. The pore sizes varied depending on the degree of cross-linking. The NBS-4 bilayer nanofibrous-hydrogel scaffold exhibited a higher porosity than all other bilayer nanofibrous hydrogels. It can be attributed to the structural integrity of NBS-4 due to the maximum cross-linking and nanofibrous phase of BS-PVA. The cross-sectional morphology of the bilayer nanofibrous hydrogels also showed porous structures with strongly interconnected pores and uniform pore size distribution (Figure 3 (i−l)). The bilayer design is essential because the two layers synergize to impart stability, controlled biodegradability, biocompatibility, hydrophilicity, porosity, and

https://doi.org/10.1021/acsomega.3c06613
ACS Omega 2024, 9, 6527−6536

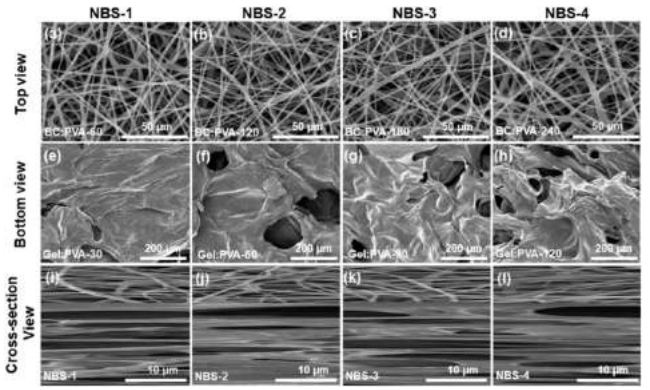

Figure 3. SEM morphology of bilayer hydrogel-nanofibrous scaffolds. The top layer is nanofiber (a–d) as analyzed at 50 μm, the bottom layer is porous hydrogel (e–h) as studied at 200 μm, and a cross-sectional view of the nanofibrous bioscaffolds (i–l) observed at 10 μm.

surface roughness to the structure, which are critical parameters for an advanced scaffold that mimics the structure of ECM to improve cell behavior and healing of soft tissue.[5]

4.4. Wetting Analysis. A biomaterial must be sufficiently hydrophilic to ensure good cell viability as this promotes cell adhesion and accelerate cell migration. Figure 4(a–d) shows the wettability of the bilayer hydrogel-nanofibrous scaffolds. The results show that all the bilayer hydrogel-nanofibrous scaffolds exhibit good wettability and hydrophilic behavior. However, hydrophilicity decreased with increasing cross-linker concentration (highest for NBS1 and lowest for NBS4). The good wettability and hydrophilic behavior of the bilayer hydrogel-nanofibrous scaffolds despite increased cross-linker concentration is due to the hydrophilic functionalities of their components (gelatin, BC, PVA, and, to some extent, the cross-linker). As mentioned earlier, adequate wettability provides a better cell adhesion and proliferation environment. It protects the wound from severe infections caused by pathogens due to its good adsorption and absorption capacity.[24] The bilayer hydrogel-nanofibrous scaffolds have shown good adsorption and absorption capabilities, reflected in the good antibacterial activity of the scaffolds (discussed in detail in a later section).[25] Therefore, it can be concluded that the synergy of bilayer hydrogel-nanofibrous scaffolds represents a future material for biomedical engineering applications.

4.5. Swelling Analysis. A better wound dressing material allows better absorption of wound exudate from the wound site.[26] Since biofluid is a mixture of several components, we used three media in the swelling analysis to evaluate the swelling capacity and behavior of the bilayer hydrogel-nanofibrous scaffolds.[27] Figure 4(e–g) shows the swelling analysis of the bilayer hydrogel-nanofibrous scaffolds at 37 °C in aqueous, PBS, and NaCl media. It is known from the literature that BC is less hydrophilic compared to gelatin, so the nanofiber component over the hydrogel exhibits lower swelling. Due to the high absorption affinity of gelatin, most of the liquid is absorbed by the porous hydrogel. As mentioned earlier, increasing the degree of cross-linking decreases the swelling ability of the bilayer hydrogel-nanofibrous nanofiber scaffolds.[28] As shown, the bilayer hydrogel-nanofibrous scaffold NBS-1 (less cross-linked sample) exhibited maximum swelling in all media (in the order Aq. > PBS > NaCl) compared to

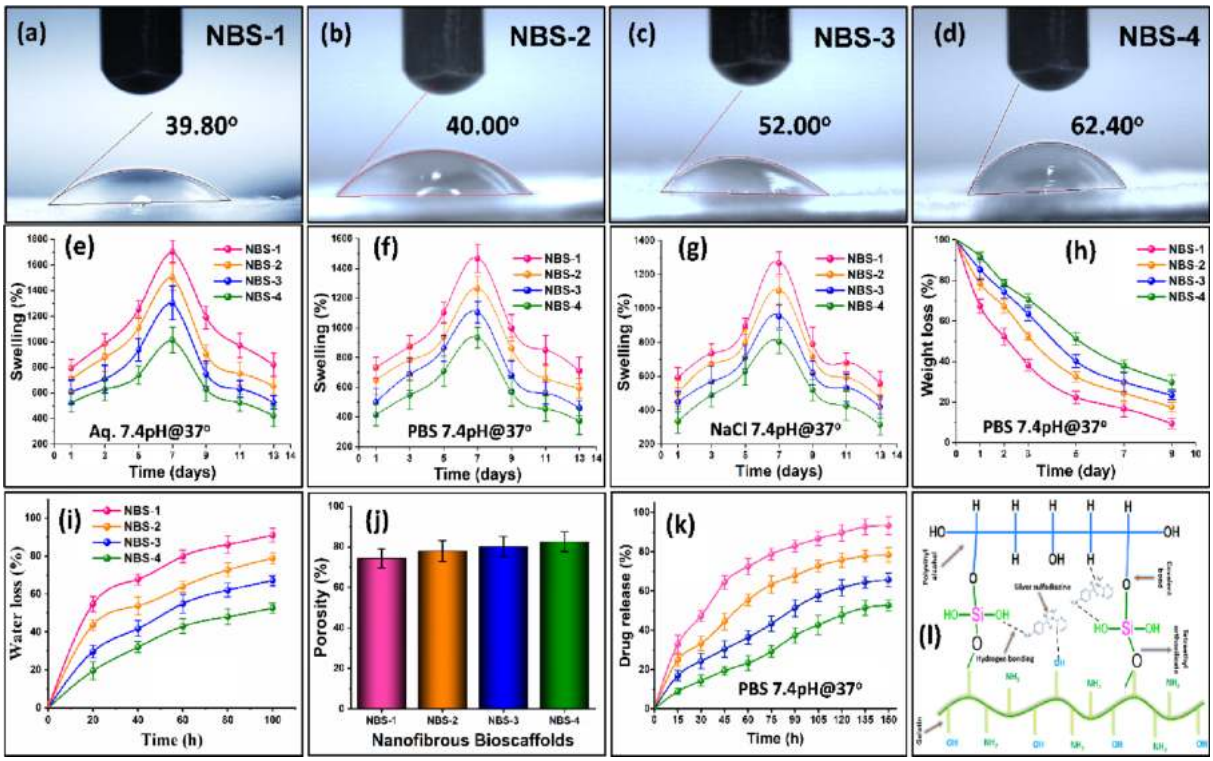

Figure 4. Physicochemical study of the bilayer hydrogel-nanofibrous scaffolds. The wetting at room temperature (a–d), the swelling in different media including aqueous, PBS, and NaCl 7.4 pH media at 37 °C (e–g), degradation in PBS media at 37 °C (h), water retention analysis in aqueous media at 37 °C (i), porosity via water displacement method in deionized double water media at room temperature (j), drug release assay in PBS media at 37 °C of bilayer hydrogel-nanofibrous scaffolds (k), and silver sulfadiazine interaction with polymeric matrix(l).

https://doi.org/10.1021/acsomega.3c06613
ACS Omega 2024, 9, 6527–6536

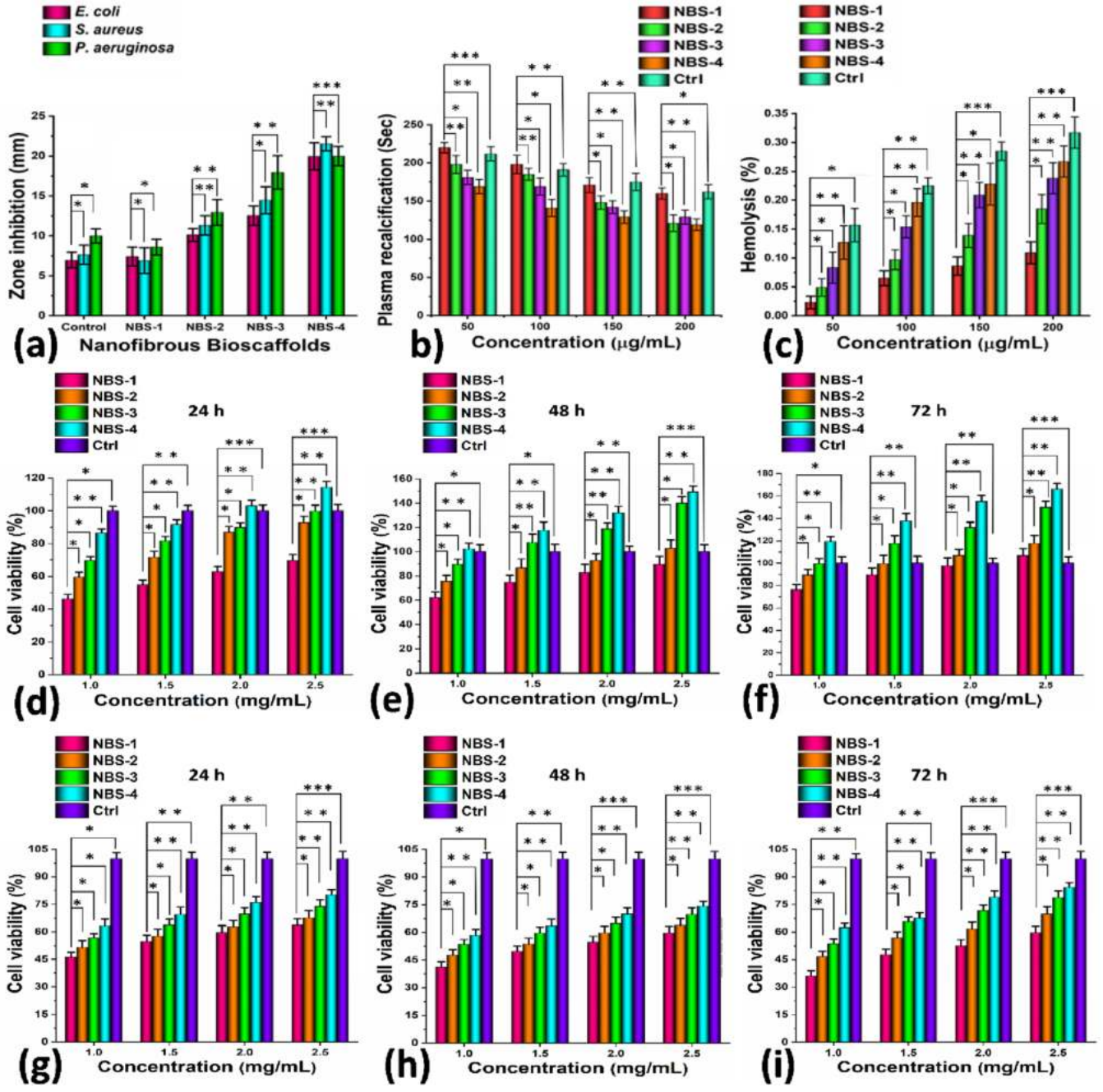

Figure 5. Antibacterial, hemocompatibility, and cell viability behavior of the nanofibrous-hydrogel materials were performed to determine their biological properties. Antibacterial activities of (a) hemocompatibility valuation by (b) plasma rectification and (c) a hemolysis assay. The cell viability of *3T3* (d−f) and *HEK-293* (g−i) cell lines against different concentrations of bilayer hydrogel-nanofibrous materials after different time intervals (24, 48, and 72 h).

NBS-4 (more cross-linked sample). However, due to its sufficient structural integrity, NBS-4 maintained its morphology and 3D architecture throughout the studies.

4.6. Degradation. The degradation of the bilayer nanofibrous scaffolds was studied in a PBS solution at 37 °C to determine their degradation at the wound site. Figure 4(h) shows sustained and controlled degradation of the bilayer nanofibrous scaffolds, although the bilayer nanofibrous scaffold NBS-1 showed faster degradation than NBS-4 due to the different degrees of cross-linking. The NBS-1 bilayer nanofibrous scaffold has the lowest cross-linking degree among all bilayer samples. The weight loss was observed due to the porous hydrogel, and the nanofibrous part of BC: PVA-120 can also degrade easily due to the bond break between BC and PVA. However, as the cross-linking degree increased, the weight loss of the bilayer nanofibrous scaffold NBS-4 decreased significantly. The weight losses of NBS-1 and NBS-4 were about 80% and 45%, respectively, after 5 days. It indicates that the NBS-4 bilayer nanofibrous scaffold is a potential wound dressing material with structural integrity that promotes wound healing without causing severe infections. It also shows that dressings can be changed every 5 days to avoid pathogenic and antibacterial activities due to dressing degradation.[29] The water retention behavior of the nanofibrous bilayer scaffold is

https://doi.org/10.1021/acsomega.3c06613
ACS Omega 2024, 9, 6527−6536

different for all the samples, the water loss was reduced with increasing degree of crosslinking that may provide desiable structural properties for water retention. The water retention was found to be maximum for NBS-4 and minimumleast for NBS-1 as shown as in Figure 4(i). From the result, it can be concluded that bilayer nanofibrous scaffolds with controlled degradation are potential wound dressing materials for wound healing and tissue engineering applications.

4.7. Porosity. The exchange of gases, nutrients, and waste products through the pores of the dressing material is one of the most important processes in wound healing. The porous biomaterial improves fibroblast adhesion, proliferation and mobility, micronutrient exchange, therapeutic agent delivery, and exudate absorption capacity at the wound site. The bilayer nanofibrous scaffolds NBS-1, NBS-2, NBS-3, and NBS-4 (Figure 4(j)) show little change in porosity, which can be attributed to the structural integration associated with the degree of cross-linking. Compared to the bilayer nanofibrous scaffolds NBS-1, NBS-2, and NBS-3, NBS-4 exhibited the highest porosity, which can be attributed to a higher degree of structural integration. The lower porosity of NBS-1, NBS-2, and NBS-3 is attributed to the lower structural integration. In these bilayer nanofibrous scaffolds, the structure fuses during their faster degradation. Therefore, NBS-4, with structural integrity and interconnected porosity, would be a potential wound dressing material for tissue engineering and wound healing. The percentage of porosity is between 70% and 80%. Therefore, a wound dressing with a 60−90% porosity range supports improved cell behavior and significant exchange of biomolecules, proteins, and growth factors for fibroblast proliferation and migration during wound healing.

4.8. In Vitro Assay. *4.8.1. Drug Release.* The drug release study from nanofibrous scaffolds in PBS medium under in vitro conditions (pH 7.4 and 37 °C) is shown in Figure 4 (k). Since the bilayer nanofibrous scaffolds are a bilayer matrix of nanofibers and porous hydrogels, the porous hydrogel contains a bioactive molecule (Ag-sulfadiazine) that acts on the wound site upon contact. The bilayer nanofibrous scaffolds allow for sustained and controlled release of Ag-sulfadiazine by absorbing biofluid and forming a preventive antibacterial zone at the host wound site. Ag-sulfadiazine was rapidly released in bilayer nanofibrous scaffolds NBS-1 and NBS-2, while sustained and controlled drug release was observed in NBS-3 and NBS-4. These release patterns are attributed to the structural integration associated with the degree of cross-linking. The sustained and controlled release in NBS-3 and NBS-4 is also attributed to their optimized hydrophilicity. The sustained and controlled release of Ag-sulfadiazine from the bilayer matrix could form a protective antibacterial zone that promotes healing through prolonged drug release and is a desirable biomaterial for tissue engineering and wound healing applications.[30]

4.8.2. Antibacterial Activities. The antibacterial potential of the bilayer nanofibrous scaffolds was investigated against Gram-positive and Gram-negative bacterial pathogens. The antibacterial active nanofibrous scaffolds can form an antibacterial zone at the wound site to determine the best formulation of the biomaterial for wound dressings (Figure 5(a)). The bilayer nanofibrous scaffolds showed better bacterial activities against Gram + ive and Gram−ive than the control group. The order of antibacterial activities was NBS-1 < NBS-2 < NBS-3 < NBS-4. The polymeric matrix containing Ag-sulfadiazine has a potential antibacterial effect that can interact with bacterial membranes. The bacterial outer layer comprises phospholipids and lipopolysaccharides, and lipopolysaccharides have a strong negative surface charge.[31] The release of the Ag-sulfadiazine interacts with the bacterial membrane and controls bacterial growth.[32,33] It was favored by the presence of TEOS, which not only separates the polymer molecules, reduces their intermolecular bonding, and makes them available for interaction with bacterial membranes but also the silicate moiety may have contributed to killing the bacteria.

4.8.3. Hemocompatibility. Studying the hemocompatibility of any major biomaterial helps determine the response to stop hemorrhage and hemolysis. Blood is a complex biofluid consisting of 1% leukocytes and platelets, 44% erythrocytes, and 55% plasma. Therefore, adverse interactions between newly developed materials and blood should be analyzed in detail to prevent the activation and destruction of the blood components. In vitro, hemocompatibility of the bilayer nanofibrous hydrogel scaffolds was performed with fresh human blood using different concentrations (50−200 μg/mL) of the bilayer nanofibrous scaffolds. Since the hemolysis rate of all hydrogels is less than 0.5%, all hydrogels are hemocompatible (Figure 5(c)).[34] In addition to hemocompatibility, the blood coagulation properties of the bilayer nanofibrous hydrogel scaffolds were also investigated (Figure 5(b)). It was found that the blood clotting time decreased with increasing cross-linking. The best clotting time was obtained for the bilayer nanofibrous scaffold NBS-4. The results clearly show that these bilayer hydrogel scaffolds are inherently hemocompatible and could be the best wound dressing material for wound healing in skin tissue engineering.

4.8.4. Cell Viability. Cell viability and proliferation are critical for any biomaterial; our nanofiber bioconstruction should meet these criteria. Cell morphology and cell viability of 3T3 and HEK-293 cell lines were examined under standard in vitro conditions after 24, 48, and 72 h to determine their cellular behavior. The bilayer nanofiber scaffolds were also used to study cell viability at different intervals to achieve prolonged cell viability. The cell viability of 3T3 (Figure 5 (d−f)) and HEK-293 (Figure 5 (g−i)) cell lines was examined at different time intervals (24, 48, and 72 h) with different concentrations of the bilayer nanofibrous scaffolds, respectively. The 3T3 cell lines exhibited increased cell viability with increasing time from 24 to 72 h and increasing concentration of the homogenized bilayer nanofibrous scaffolds (Figure 5(d−f)). The HEK-293 cell lines also showed increased cell viability with increasing time intervals from 24 to 72 h and increasing concentration of the bilayer nanofibrous scaffolds (Figure 5(g−i)). The results suggest that bilayer nanofibrous scaffolds significantly promote cell adhesion and growth, enhance cell−cell interaction, and stimulate cell proliferation and seeding.[35,36]

4.8.5. Cell Morphology. All samples showed desirable cell growth with a regulated cylindrical morphology for the 3T3 cell lines (Figure 6(a)).[37] It can also be observed that the cell morphology and density increased initially with increasing time from 24 to 72 h. The bilayer nanofibrous scaffolds could provide sufficient activated sites for cell adhesion, which promotes cell growth. Accordingly, the HEK-293 cell lines showed similar cellular behaviors, and it can be observed that they increased with increasing time from 24 to 72 h (Figure 6(b)) and began to interact with neighboring cells to form clusters or small groups by interacting with their membranes.

https://doi.org/10.1021/acsomega.3c06613
ACS Omega 2024, 9, 6527−6536

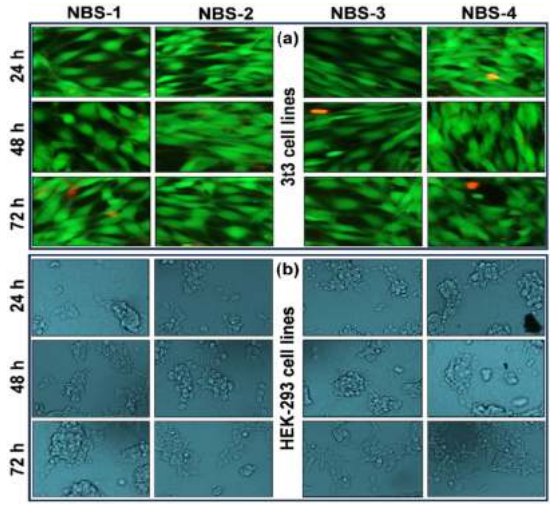

Figure 6. Cell morphology of fibroblast (a) and human embryonic kidney (b) cell lines on bilayer hydrogel-nanofibrous materials after different time intervals (24, 48, and 72 h) to determine the cellular behavior.

The behavior of HEK-293 cell lines confirmed that the fabricated material promoted vascularization and tissue repair and regeneration activities of the injury or wound.

5. CONCLUSIONS

Tissue engineering is the fastest-growing field, requiring the production of advanced and functional materials that can be used as scaffolds or dressings for tissue regeneration. This study presents a bilayer material prepared by electrospinning a PVA-containing BC-NFs hybrid material (top layer) over a highly interconnected porous 3D gelatin-PVA hydrogel (bottom layer) obtained by freeze-drying. The techniques were combined to produce an advanced material with synergistic effects on the physical and biological properties of both materials. FT-IR confirmed the cross-linking of the top and bottom layers, and SEM showed a porous structure of the bottom layer, random deposition of NFs on the surface, and aligned NFs in the cross section. The bilayer hybrid material demonstrated a hydrophilic surface, high swelling ability, good stability, and adequate porosity. In addition, the bilayer material released Ag-sulfadiazine in a sustained and controlled manner and showed good antibacterial activities against severe disease-causing Gram+ive and Gram−ive (*E. coli*, *S. Aureus*, and *P. Aeruginosa*) bacterial strains. In vitro biological studies were performed on *3T3* and *HEK-293* cell lines, showing good hemocompatibility and desirable cell viability, proliferation, and adhesion to the bilayer material. Thus, the synergistic effect of NFs and hydrogel resulted in a potential wound dressing material for wound healing and soft tissue engineering.

AUTHOR INFORMATION

Corresponding Authors

Muhammad Umar Aslam Khan − *Biomedical Research Center, Qatar University, Doha 2713, Qatar; Department of Mechanical and Industrial Engineering, Qatar University, Doha 2713, Qatar; BioInspired Device and Tissue Engineering Research Group, School of Biomedical Engineering and Health Sciences, Faculty of Engineering, Universiti Teknologi Malaysia, Skudai, Johor 81300, Malaysia;* orcid.org/0000-0001-8105-2651; Email: umar007khan@gmail.com

Saiful Izwan Abd Razak − *BioInspired Device and Tissue Engineering Research Group, School of Biomedical Engineering and Health Sciences, Faculty of Engineering and Sports Innovation & Technology Centre, Institute of Human Centred Engineering, Universiti Teknologi Malaysia, Skudai, Johor 81300, Malaysia*; Email: saifulizwan@utm.my

Authors

Rawaiz Khan − *Faculty of Chemical and Energy Engineering, Universiti Teknologi Malaysia (UTM), Johor Bahru, Johor 81310, Malaysia*

Goran M. Stojanović − *Department of Electronics, Faculty of Technical Sciences, University of Novi Sad, Novi Sad 21000, Serbia*

Aneela Javed − *Department of Healthcare Biotechnology, Atta Ur Rahman School of Applied Biosciences, National University of Sciences and Technology, Islamabad 44000, Pakistan;* orcid.org/0000-0003-0280-0610

Sajjad Haider − *Chemical Engineering Department, College of Engineering, King Saud University, Riyadh 11421, Saudi Arabia*

Complete contact information is available at: https://pubs.acs.org/10.1021/acsomega.3c06613

Author Contributions

M.U.A.K., R.K., and S.H. contributed to conceptualization; M.U.A.K., R.K., and G.M.S. contributed to data curation; M.U.A.K., R.K., and S.H. contributed to formal analysis; M.U.A.K. and G.M.S. contributed to funding acquisition; M.U.A.K., S.H., and S.I.A.R. contributed to investigation; R.K., M.U.A.K. and G.M.S. contributed to methodology; M.U.A.K., G.M., and S.H. contributed to project administration; M.U.A.K. and G.M.S. contributed to resources; M.U.A.K. and R.K. contributed to software; M.U.A.K., S.I.A.R., and S.H. contributed to supervision; G.M.S., S.H., and S.I.A.R. contributed to validation; M.U.A.K. contributed to visualization; M.U.A.K. and R.K. contributed to Writing−original draft; M.U.A.K., R.K., and S.H. contributed to writing−review and editing.

Notes

The authors declare no competing financial interest.

ACKNOWLEDGMENTS

We would like to thank the European Union's Horizon programme for partly supporting the research project. This project has received funding from the European Union's Horizon 2020 Research and Innovation Program under grant agreement no. 872370.

REFERENCES

(1) Khan, M. U. A.; Abd Razak, S. I.; Haider, S.; Mannan, H. A.; Hussain, J.; Hasan, A. Sodium alginate-f-GO composite hydrogels for tissue regeneration and antitumor applications. *Int. J. Biol. Macromol.* **2022**, *208*, 475−485.

(2) Monika, P.; Chandraprabha, M. N.; Rangarajan, A.; Waiker, P. V.; Chidambara Murthy, K. N. Challenges in healing wound: Role of complementary and alternative medicine. *Front. Nutr.* **2022**, *8*, 791899.

(3) Khan, M. U. A.; Stojanović, G. M.; Hassan, R.; Anand, T. J. S.; Al-Ejji, M.; Hasan, A. Role of Graphene Oxide in Bacterial Cellulose−

Gelatin Hydrogels for Wound Dressing Applications. *ACS Omega* **2023**, *8* (18), 15909−15919.
(4) Abdollahiyan, P.; Oroojalian, F.; Mokhtarzadeh, A. The triad of nanotechnology, cell signalling, and scaffold implantation for the successful repair of damaged organs: An overview on soft-tissue engineering. *J. Controlled Release* **2021**, *332*, 460−492.
(5) Behere, I.; Ingavle, G. In vitro and in vivo advancement of multifunctional electrospun nanofiber scaffolds in wound healing applications: Innovative nanofiber designs, stem cell approaches, and future perspectives. *J. Biomed. Mater. Res., Part A* **2022**, *110* (2), 443−461.
(6) Zhong, Y.; Xiao, H.; Seidi, F.; Jin, Y. Natural polymer-based antimicrobial hydrogels without synthetic antibiotics as wound dressings. *Biomacromolecules* **2020**, *21* (8), 2983−3006.
(7) Khan, M. U. A.; Abd Razak, S. I.; Rehman, S.; Hasan, A.; Qureshi, S.; Stojanović, G. M. Bioactive scaffold (sodium alginate)-g-(nHAp@ SiO_2@ GO) for bone tissue engineering. *Int. J. Biol. Macromol.* **2022**, *222*, 462−472.
(8) Khan, M. U. A.; Aslam, M. A.; Abdullah, M. F. B.; Hasan, A.; Shah, S. A.; Stojanović, G. M. Recent perspective of polymeric biomaterial in tissue engineering−a review. *Mater. Today Chem.* **2023**, *34*, 101818.
(9) Kang, J. I.; Park, K. M. Advances in gelatin-based hydrogels for wound management. *J. Mater. Chem. B* **2021**, *9* (6), 1503−1520.
(10) Khan, M. U. A.; Al-Arjan, W. S.; Ashammakhi, N.; Haider, S.; Amin, R.; Hasan, A. Multifunctional bioactive scaffolds from ARX-g-(Zn@ rGO)-HAp for bone tissue engineering: In vitro antibacterial, antitumor, and biocompatibility evaluations. *ACS Appl. Bio Mater.* **2022**, *5* (11), 5445−5456.
(11) Khan, M. U. A.; Stojanović, G. M.; Abdullah, M. F. B.; Dolatshahi-Pirouz, A.; Marei, H. E.; Ashammakhi, N.; Hasan, A. Fundamental properties of smart hydrogels for tissue engineering applications: A review. *Int. J. Biol. Macromol.* **2023**, *254*, 127882.
(12) Rasouli, M.; Soleimani, M.; Hosseinzadeh, S.; Ranjbari, J. Bacterial cellulose as potential dressing and scaffold material: toward improving the antibacterial and cell adhesion properties. *J. Polym. Environ.* **2023**, *31*, 4621−4640.
(13) Khan, M. U. A.; Stojanović, G. M.; Rehman, R. A.; Moradi, A.-R.; Rizwan, M.; Ashammakhi, N.; Hasan, A. Graphene Oxide-Functionalized Bacterial Cellulose−Gelatin Hydrogel with Curcumin Release and Kinetics: In Vitro Biological Evaluation. *ACS Omega* **2023**, *8* (43), 40024−40035.
(14) Ijaola, A. O.; Akamo, D. O.; Damiri, F.; Akisin, C. J.; Bamidele, E. A.; Ajiboye, E. G.; Berrada, M.; Onyenokwe, V. O.; Yang, S.-Y.; Asmatulu, E. Polymeric biomaterials for wound healing applications: A comprehensive review. *J. Biomater. Sci., Polym. Ed.* **2022**, *33* (15), 1998−2050.
(15) Khan, M. U. A.; Razak, S. I. A.; Hassan, A.; Qureshi, S.; Stojanović, G. M.; Ihsan-Ul-Haq. Multifunctional arabinoxylan-functionalized-graphene oxide based composite hydrogel for skin tissue engineering. *Front. Bioeng. Biotechnol.* **2022**, *10*, 865059.
(16) Iuchi, K.; Oya, K.; Hosoya, K.; Sasaki, K.; Sakurada, Y.; Nakano, T.; Hisatomi, H. Different morphologies of human embryonic kidney 293T cells in various types of culture dishes. *Cytotechnology* **2020**, *72*, 131−140.
(17) Kouser, R.; Vashist, A.; Zafaryab, M.; Rizvi, M. A.; Ahmad, S. Biocompatible and mechanically robust nanocomposite hydrogels for potential applications in tissue engineering. *Mater. Sci. Eng., C* **2018**, *84*, 168−179.
(18) Plange, P. N. A.; Aikins, A. R.; Brobbey, K. J.; Kaufmann, E. E. Cassava microfiber−reinforced gelatin scaffold holds promise for tissue engineering by exhibiting cytocompatibility with HEK 293 cells. *Exp. Biol. Med.* **2023**, *248*, 936−947.
(19) Repetto, G.; Del Peso, A.; Zurita, J. L. Neutral red uptake assay for the estimation of cell viability/cytotoxicity. *Nat. Protoc.* **2008**, *3* (7), 1125−1131.
(20) Sari, M.; Hening, P.; Chotimah; Ana, I. D.; Yusuf, Y. Bioceramic hydroxyapatite-based scaffold with a porous structure using honeycomb as a natural polymeric Porogen for bone tissue engineering. *Biomater. Res.* **2021**, *25* (1), 1−13.
(21) Tomar, P.; Kumar, R.; Lakhani, R.; Srivastava, A.; Chhibber, V. K. Improvement in hygroscopic property of macro-defect free cement modified with hypromellose/potassium methyl siliconate copolymer and pulverized fly ash. *J. Therm. Anal. Calorim.* **2022**, *147* (22), 12417−12430.
(22) Zheng, W.; Xu, C.-H. Innovative Approaches and Advances for Hair Follicle Regeneration. *ACS Biomater. Sci. Eng.* **2023**, *9* (5), 2251−2276.
(23) Amani, H.; Arzaghi, H.; Bayandori, M.; Dezfuli, A. S.; Pazoki-Toroudi, H.; Shafiee, A.; Moradi, L. Controlling cell behavior through the design of biomaterial surfaces: A focus on surface modification techniques. *Adv. Mater. Interfaces* **2019**, *6* (13), 1900572.
(24) Gao, Y.; Qiu, Z.; Liu, L.; Li, M.; Xu, B.; Yu, D.; Qi, D.; Wu, J. Multifunctional fibrous wound dressings for refractory wound healing. *J. Polym. Sci.* **2022**, *60* (15), 2191−2212.
(25) Huang, Y.; Bai, L.; Yang, Y.; Yin, Z.; Guo, B. Biodegradable gelatin/silver nanoparticle composite cryogel with excellent anti-bacterial and antibiofilm activity and hemostasis for Pseudomonas aeruginosa-infected burn wound healing. *J. Colloid Interface Sci.* **2022**, *608*, 2278−2289.
(26) Liu, H.; Wang, C.; Li, C.; Qin, Y.; Wang, Z.; Yang, F.; Li, Z.; Wang, J. A functional chitosan-based hydrogel as a wound dressing and drug delivery system in the treatment of wound healing. *RSC Adv.* **2018**, *8* (14), 7533−7549.
(27) Mohan, T.; Dobaj Štiglic, A.; Beaumont, M.; Konnerth, J.; Gürer, F.; Makuc, D.; Maver, U.; Gradišnik, L.; Plavec, J.; Kargl, R.; Kleinschek, K. S. Generic method for designing self-standing and dual porous 3D bioscaffolds from cellulosic nanomaterials for tissue engineering applications. *ACS Appl. Bio Mater.* **2020**, *3* (2), 1197−1209.
(28) Wang, S.; Li, K.; Zhou, Q. High strength and low swelling composite hydrogels from gelatin and delignified wood. *Sci. Rep.* **2020**, *10* (1), 17842.
(29) Yu, R.; Zhang, H.; Guo, B. Conductive biomaterials as bioactive wound dressing for wound healing and skin tissue engineering. *Nanomicro lett.* **2022**, *14*, 1−46.
(30) Liu, X.; Fan, H.; Meng, Z.; Wu, Z.; Gu, R.; Zhu, X.; Gan, H.; Dou, G. Combined silver sulfadiazine nanosuspension with thermosensitive hydrogel: An effective antibacterial treatment for wound healing in an animal model. *Int. J. Nanomed.* **2023**, *18*, 679−691.
(31) Paracini, N.; Schneck, E.; Imberty, A.; Micciulla, S. Lipopolysaccharides at solid and liquid interfaces: Models for biophysical studies of the gram-negative bacterial outer membrane. *Adv. Colloid Interface Sci.* **2022**, *301*, 102603.
(32) Bazmandeh, A. Z.; Mirzaei, E.; Fadaie, M.; Shirian, S.; Ghasemi, Y. Dual spinneret electrospun nanofibrous/gel structure of chitosan-gelatin/chitosan-hyaluronic acid as a wound dressing: In-vitro and in-vivo studies. *Int. J. Biol. Macromol.* **2020**, *162*, 359−373.
(33) Khan, M. U. A.; Stojanović, G. M.; Hassan, R.; Sahaya Anand, T. J.; Al-Ejji, M.; Hasan, A. Graphene oxide role in Bacterial cellulose/gelatin crosslinked hydrogels for wound dressing applications. *ACS Omega* **2023**, *18*, 15909−15919.
(34) Ooi, C.-H.; Ling, Y. P.; Abdullah, W. Z.; Mustafa, A. Z.; Pung, S.-Y.; Yeoh, F.-Y. Physicochemical evaluation and in vitro hemocompatibility study on nanoporous hydroxyapatite. *J. Mater. Sci.: Mater. Med.* **2019**, *30*, 1−10.
(35) Cui, H.; Wang, W.; Shi, L.; Song, W.; Wang, S. Superwettable surface engineering in controlling cell adhesion for emerging bioapplications. *Small Methods* **2020**, *4* (12), 2000573.
(36) Badhe, R. V.; Chatterjee, A.; Bijukumar, D.; Mathew, M. T. Current advancements in bio-ink technology for cartilage and bone tissue engineering. *Bone* **2023**, *171*, 116746.
(37) Li, Y.; Zhong, Z.; Xu, C.; Wu, X.; Li, J.; Tao, W.; Wang, J.; Du, Y.; Zhang, S. 3D micropattern force triggers YAP nuclear entry by transport across nuclear pores and modulates stem cells paracrine. *Natl. Sci. Rev.* **2023**, *10*, nwad165.

https://doi.org/10.1021/acsomega.3c06613
ACS Omega 2024, 9, 6527−6536